Photothermal studies of single molecules and gold nanoparticles : vapor nanobubbles and conjugated polymers

Hou, L.

3

Explosive formation and dynamics of vapor nanobubbles around a continuously heated gold nanosphere

Abstract– *We form sub-micrometer-sized vapor bubbles around a single laser-heated gold nanoparticle in a liquid and monitor those through optical scattering of a probe laser. Bubble formation is explosive even under continuous-wave heating. The fast, inertia-governed expansion is followed by a somewhat slower contraction and disappearance after some tens of nanoseconds. In a narrow range of illumination powers, bubble time traces show a clear echo signature. We attribute it to sound waves released upon the initial explosion and reflected by flat interfaces, hundreds of microns away from the particle. Echoes can trigger new explosions. A nanobubble's steady state (with a vapor shell surrounding the heated nanoparticle) can be reached by a proper time profile of the heating intensity. Stable nanobubbles could have original applications for light modulation and for enhanced optical-acoustic coupling in photoacoustic microscopy.*

The contents of this chapter are based on:
L. Hou, M. Yorulmaz, N.R. Verhart and M. Orrit. *"Explosive formation and dynamics of vapor nanobubbles around a continuously heated gold nanosphere"*. New J. Phys. **17**, 013050 (2015).

3.1. Introduction

Gas bubbles in liquids are involved in many processes and applications [4]. Cavitation bubbles cause mechanical damage [3], and even can produce high-energy electromagnetic radiation, an effect called sonoluminescence [5]. The dynamics of bubbles driven by acoustic waves is highly nonlinear and displays many complex phenomena including chaos [4]. In the present chapter, we consider nanobubbles, i.e., bubbles with diameters of a few tens to hundreds of nanometers. Compared to earlier experiments on microbubbles (a few microns to tens of microns in diameter), nanobubbles are more difficult to observe, study and manipulate. However, they may give rise to simpler or different properties, for example because liquid flows around nanobubbles present lower Reynolds numbers [16].

The standard method to form a gas bubble optically is to illuminate an absorbing liquid with a (sub-)picosecond laser pulse [69, 70]. Alternatively, the energy absorbed by a metal nanoparticle is transferred to the liquid by conduction. Because of the fast excitation and of the high heat conductivity of the metal, the particle's temperature is raised within a few picoseconds to well above the boiling temperature of the liquid, whose sudden vaporization leads to a necessarily explosive expansion of hot steam, pushing the liquid away and launching bubble dynamics in the nanosecond time regime. Transient nanobubbles produced by short laser pulses have been monitored [25, 31, 71] i) by optical imaging with short pulses, giving direct access to bubble size, ii) through the time dependence of probe light scattered off the bubble, giving time-resolved information, iii) by acoustic detection of emitted sound waves [25], or by the combination of electric conductivity through a nanopore and optical detection [28]. The environment change upon boiling can be detected via the particle's plasmon resonance [39], or by photothermal detection [72] but with limited time resolution. Ensembles of nanobubbles were studied by light scattering and by small-angle X-ray scattering of short X-ray pulses [32], or by pump-probe spectroscopy [73, 74], but these methods do not apply to single nanobubbles. Baffou *et al.* [75] used an imaging microscope to create microbubbles with continuous illumination of a single gold nanoparticle, also with low time resolution. Cichos' group modulated a probe beam by an isotropic bubble in a nematic liquid crystal close to its phase transition [76], but this process is much slower than the liquid-vapor equilibria considered here.

Stable nanobubbles are interesting for their fundamental properties [77, 78] and may have useful applications [79]. A nanobubble is an efficient two-way transducer between acoustic and optical waves because of its large compressibility and optical scattering cross-section. A stable nanobubble could be an

attractive beacon, source, or detector in photoacoustic microscopy [80].

Thus, we set out to heat a gold nanoparticle with a continuous laser beam, striving towards a precise balance between heat production in the nanoparticle and heat loss to the surrounding liquid. We monitor bubble formation and dynamics optically, which provides high time resolution down to the nanosecond, single-shot regime. Future experiments with short probe pulses and stroboscopic detection may give access to the sub-picosecond regime. To our surprise, we could not pass continuously from regime I where the particle is surrounded by hot liquid to regime II where a stable vapor shell is present around the particle, by increasing the heating power (see Chapter 2 for details). Instead, the system undergoes an explosive transition. After characterizing this instability, we show that a proper time profile of the heating intensity allows us to create a persistent nanobubble that lasts up to a microsecond.

3.2. Methods and experimental details

One of our main concerns is the reproducibility of our experiments. We wanted to study the same nanoparticle for a long time under different experimental conditions for direct comparison. We therefore worked with gold nanospheres immobilized on a glass substrate, which can be imaged with high precision in a standard confocal microscope. To obtain large enough optical signals, the size of nanoparticles was chosen to be 80 nm in diameter. We also expect surface effects and irreversible shape changes of the particle or of the particle-substrate area to be (relatively) less important for large particles. The gold colloidal suspension is bought from a commercial company (British Biocell International). The diameter of the particle is about 78 nm on average with 4.5 nm standard deviation (see Fig.3.1.b).

For the sample preparation, we used gold nanospheres and immobilized these on a glass coverslip by spin coating. The particles and the glass substrates were cleaned from organic ligands by repeated flushing and ozone cleaning. We checked that all particles used in the present work were isolated single ones, by photothermal contrast [81]. The particles were covered with the liquid (water or n-pentane), so that bubbles could form in the half-space limited by the flat glass-liquid interface. This breaks the spherical symmetry of the nanobubble with respect to the gold nanoparticle and the interface (see the scheme in Fig.3.1.a), but the nanobubble itself could have a spherical shape. Our first experiments were done in water for convenience and because it is by far the most interesting fluid for applications. However, boiling water around a nanoparticle requires temperatures up to 550 K, and the temperature of the gold particle can easily reach several hundreds of Kelvin above the water's temperature (see

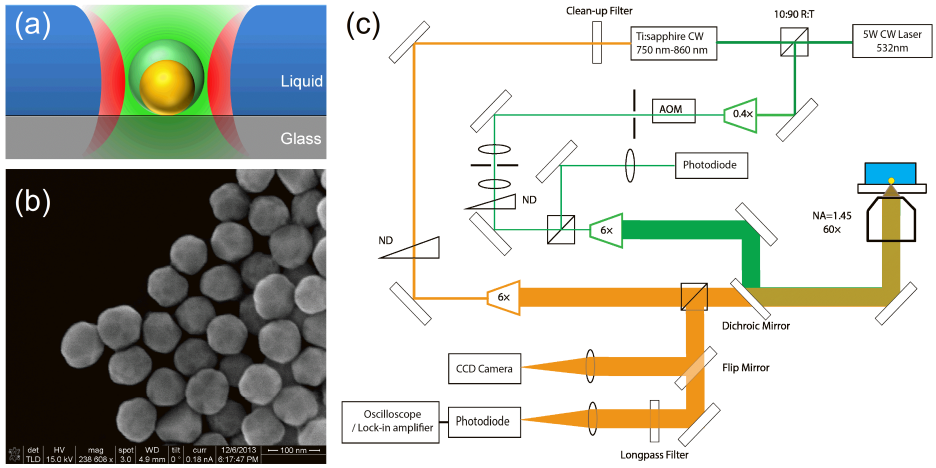

Figure 3.1: (a) Scheme of the vapor bubble formation; (b) SEM image of 80 nm gold spheres. Scale bar is 100 nm; (c) Experimental setup. AOM: acousto-optic modulator; ND: variable neutral-density filter.

Fig.2.4 in Chapter 2). Such high temperatures can lead to irreversible changes in particle shape (movement of facets and of surface atoms) and, more critically, to changes in the contact area between gold and glass. Therefore, to limit the possibility of such random or irreversible changes we used n-pentane in most experiments. Pentane has a low boiling point (309 K at atmospheric pressure), so that the estimated particle's temperature did not exceed 370 K upon boiling under our experimental conditions. This temperature remains low enough so that we can safely neglect surface rearrangements even after long illumination times.

The optical setup, shown in Fig.3.1 (c), is a typical photothermal microscope [42]. The advantages of an all-optical investigation of the nanobubble are its speed, non-invasiveness and sensitivity. Photothermal microscopy is a technique based on the absorption of small objects such as gold nanoparticles. A modulated heating beam heats the nanoparticle and creates a temperature gradient, or thermal lens, around the absorbing object. A non-resonant probe beam, which is spatially overlapped with the heating beam, is scattered by the thermal lens and interferes with a reference beam, usually the transmitted or reflected probe beam. The interfering probe beam is then collected by a photodetector such as a photodiode, and the signal is demodulated by a lock-in amplifier. We used the photothermal signal to overlap the heating (532 nm) and probe (815 nm) beams, to identify single gold nanoparticles in the sample, and also to find the critical intensity required for boiling. However, the photother-

mal signal, being produced by a lock-in amplifier with an integration time of at least 0.1 ms, was too slow to follow fast bubble kinetics in the nanosecond and microsecond domains. For those time-resolved measurements, the probe signal collected in reflection mode in bright-field scattering [82] was directly fed into the fast photodiode and the electronic signal was recorded in a fast oscilloscope with large memory.

3.3. Photothermal detection

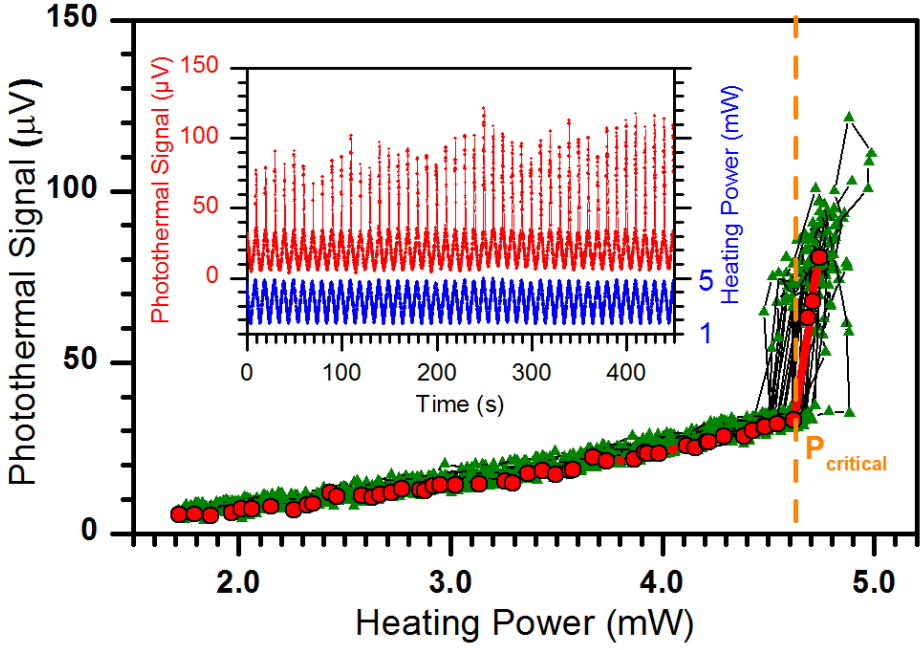

Figure 3.2: Photothermal signal of a single gold nanosphere in water as the heating intensity is increased. Until a critical power of 4.6 mW (about 0.6 MW/cm^2) the signal increases smoothly as expected for heated liquid water. Above the critical power, the signal undergoes a sudden jump to a much higher value, with large fluctuations. Red dots: a typical example of a power sweep; green triangles: accumulated data from many sweeps showing the dispersion in signal and in critical power. The data of each sweep are connected by a solid line. Insert: photothermal signal (red line, left scale) as a function of time while the heating power (blue line, right scale) is swept as a saw-tooth function between values below and above the critical power.

We started our study of single immobilized nanospheres in water with photothermal contrast. At low heating power, we find continuous heating of the liquid around the particle [83]. Above a critical pump intensity, the photothermal signal increases suddenly as shown in Fig 3.2, due to water boiling and

nanobubble formation. Repeated heating cycles around the threshold power show fluctuations of the transition power by a few percent. The particle temperature, estimated from the absorption cross section and the heat conductivity of water and glass (see Chapter 2 and Appendix C for details), corresponds well with the simple model in Chapter 2. However, this steady-state model fails to explain the strong variability of the signal and the irreproducibility of successive transitions. Even at its highest time resolution (0.1 ms) of lock-in detector, the detection is too slow to follow the dynamics of the nanobubble.

The model of Fig.2.4 in Chapter 2 shows that the particle temperature can rise by hundreds of K once the bubble forms. Such high temperatures might degrade the particle's shape and its contact area with the substrate. Therefore, we adjusted the intensity carefully to avoid damaging the particle. Moreover, we switched to a different liquid, n-pentane, which has a much lower boiling point than water, to further limit irreversible damage to the system and ensure reproducibility of the results. The physics of bubble formation and dynamics in pentane will thus serve as a model for bubble formation in water.

3.4. Direct probe detection

We directly detect the scattered probe intensity with the fast photodiode, following the bubble signal in real time. Figure 3.3 (a) shows an example of a time trace recorded at 100 μW, just above the critical power (94 μW) in liquid pentane. The complex boiling trace of Fig 3.3 (a) appears as a succession of brief and violent events lasting some tens of nanoseconds only, separated by 500 ns on average. Such violent events are characteristic of explosive boiling, which is often observed in superheated liquids [64], and which can be suppressed with superhydrophobic coatings [84]. Herein, we use the word "explosion" to describe a rapid bubble expansion on the nanosecond time scale, similar to what is customary in pulsed heating experiments [4, 13, 16, 28, 70]. Note that these explosions occur at low Reynolds numbers (defined as $Re = \rho v R_b/\mu$, where ρ and μ are the liquid density and viscosity; v and R_b are the characteristic velocity and the size of such explosions), of the order of unity. The contraction or the decay part of the nanobubble signal resembles the collapse behavior of acoustically driven gas bubbles [4]. The signal-to-noise ratio is good enough to follow individual explosions (Fig 3.3.b), which present a rise time of about 14 ± 2 ns and a decay time of about 31 ± 7 ns, longer than the detector's rise and fall times 5 and 16 ns respectably. We averaged hundreds of such events, synchronizing them with the rising edge of the signal, and obtained the averaged profile of Fig 3.3 (c), which appears only slightly broadened by the averaging to a rise time of 18 ns. The decay part of the explosion signal presents a small but reproducible

shoulder which will be discussed below. Beyond the main initial peak, the averaged trace shows further undulations at longer times, with average spacing of 500 ns, corresponding to the later explosions. They broaden with time because of the lack of exact periodicity.

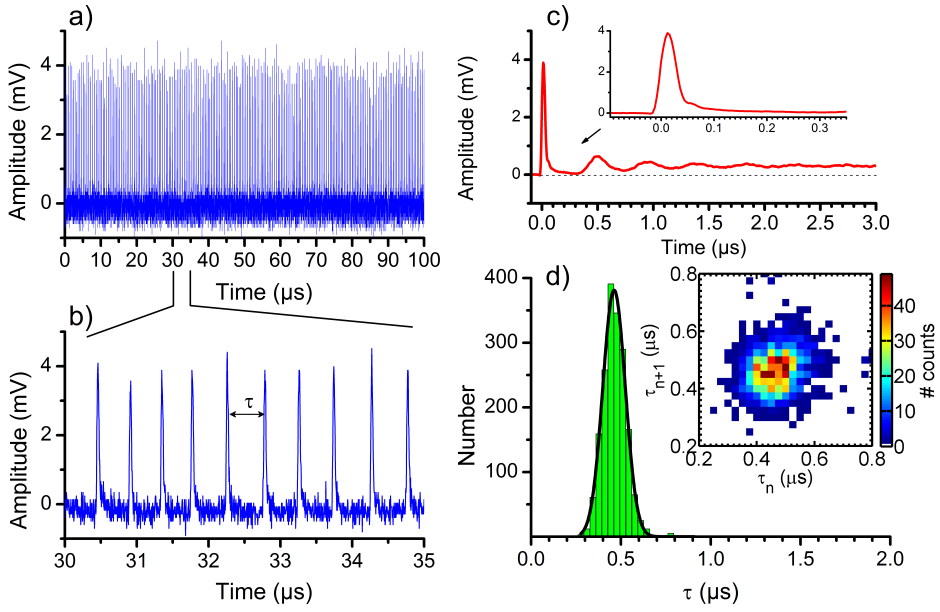

Figure 3.3: Direct probe detection of nanobubbles under constant heating (100 μW) just above the threshold for boiling. Detector gain: ×1000, bandwidth: 10 MHz. (a) Typical time trace of the scattered probe beam showing successive explosive nanobubble events. The probe power is fixed at 5 mW; (b) Further zoom-in on one part of time trace (a); (c) Average of 3,123 explosions in time trace (a), taking the half maximum of the rising edge of the signal as the time reference. Insert: zoom-in on the main peak; (d) the histogram of delay times between two successive explosions. The solid line is a Gaussian fit. Insert: scatter plot of all pairs of consecutive delays, τ_n and τ_{n+1} , from the trace in (a).

Taking a long trace with hundreds of bubble explosions, we can look at the distribution of inter-explosion delays, shown in Fig.3.3 (d). No explosion is found to occur at less than 300 ns from the previous one. The distribution is well fitted by a Gaussian, with a maximum at about 500 ns for the conditions of Fig.3.3 (d). We also present a scatter plot of the pairs of times between successive events (τ_n, τ_{n+1}) in a 2D diagram (Fig.3.3.d, insert). This plot appears compatible with a purely random succession of inter explosion times drawn at random from the Gaussian distribution of Fig.3.3 (d). We thus conclude that the random noise causing jitter, or deviations from the average inter-explosion

times, are uncorrelated between successive events. Similar jitter observations were reported in ref. [28], and attributed to randomness in the bubble nucleation process. In particular, the jitter in nanobubble dynamics is not caused by experimental imperfections such as laser intensity noise or focus drift. Note that heating intensity drifts can affect our measurements, as shown in the Appendix E.

We now propose and discuss a mechanism for this unexpected explosive boiling under continuous-wave heating conditions. As we saw in the introduction and Chapter 2, to nucleate and grow, the nanobubble needs to overcome the Laplace pressure in addition to the ambient pressure. This only happens at 367 K for an 80-nm particle in pentane (483 K in water). Once the bubble starts to grow, however, the effective boiling temperature decreases because the Laplace pressure itself decreases. When a small part of the hot liquid vaporizes, it generates a first very thin vapor shell, which pushes the remaining hot liquid just outside the bubble. This hot liquid now becomes overheated with respect to the vapor in the bubble, because of the lowered Laplace pressure. It will then feed fresh steam into the bubble, further amplifying the expansion. We have estimated the energies involved in bubble growth (see details in the Appendix D). We find three main contributions. Two of them are energy costs: i) the surface energy, which increases with bubble radius because both surface and surface tension increase, ii) the latent vaporization heat and internal vapor energy needed to expand the bubble. The third contribution is a source of energy, iii) the thermal energy stored in the overheated liquid layer. This heat can flow either to the cooler water layers at larger radii, or towards the bubble, helping its growth. For a final bubble radius of 140 nm, these contributions are - 1 fJ, -2.8 fJ, and 8.3 fJ, respectively, which indicates that bubble expansion liberates energy and is therefore thermodynamically favorable. Note that conduction through the liquid is fast enough to make this energy kinetically available during the expansion, as the diffusivity of heat in liquid pentane ($6\times10^{-8}\mathrm{m}^2/\mathrm{s}$) corresponds to 8 nm in 1 ns. Once the excess thermal energy has been consumed into surface energy and latent heat, the bubble eventually reaches a maximum radius and shrinks back under the restoring forces of surface tension and vapor condensation. Indeed, at the maximum bubble radius, cooling of the thinned hot liquid layer by the outer cold liquid is very efficient. This explains that the bubble may disappear completely upon shrinking, as the returning cold bubble wall can condensate all the vapor. The cold liquid will have to be heated again by the nanoparticle during some hundreds of nanoseconds in our conditions before a new overheated layer is established and a new explosion can take place.

We note that a similar mechanism is at work in short-pulse experiments,

where heat supplied by the hot nanoparticle first has to be conducted to the surrounding liquid before boiling can set in [32]. We can also compare our system to air bubbles in water. Those can reach very small minimal radii, with accordingly high temperatures and luminescence [85], followed by multiple afterbounces. In our case, however, the steam condensates until the bubble's surface hits the nanoparticle and the bubble disappears. Indeed, the data of Fig.3.3 (b) and Fig.3.3 (c) show that this contraction step is not followed by any clear afterbounces, apart from the small shoulder seen in Fig.3.3 (c) at 60 ns, which will be discussed hereafter. The explosion repetition rate is mainly determined by the rate at which the overheated liquid layer is heated, but it may also depend on the microscopic crossing of the nucleation barrier, as proposed recently by Nagashima et al. [28] in the bubbles produced by Joule dissipation in a nanopore. Our analysis of time traces of Fig.3.3 did not reveal any sign of a chaotic dynamics [86].

3.5. Estimation of bubble size

As the bubble is presumably smaller than the diffraction limit of the microscope, direct imaging cannot be applied. We estimated the bubble size in three independent manners:

i) From the time dependence of explosions: From published experiments [4, 25, 70] and theory [16], the bubble expansion and contraction times vary approximately linearly with bubble radius. The associated velocities are found in the range 10-15 m/s for water. The Rayleigh theory gives a similar number and ref. [25] finds that surface tension introduces a factor of about 2 with respect to Rayleigh theory. From these values and a time of about 15 ns, we estimate the bubble radius in our experiments to 150 nm.

ii) From the decreased scattered probe intensity with offset of the beam from the particle: By shifting the probe focus off the maximum overlap with the particle, we find that the signal decreases to half its value for a distance of 160 nm, which would correspond roughly to the radius of the bubble (distance of the edge to the center).

iii) From the absolute scattered probe intensity compared to reflected intensity: We compared the scattered probe intensity to the probe intensity reflected by the interface. The change upon bubble explosion is about 20%. By identifying this ratio to an area ratio between the bubble's cross section and the diffraction-limited cross section of the probe beam, we obtain a radius of about 200 nm.

Therefore, the three independent estimates above converge to a bubble radius of 100-200 nm, below the microscope's resolution.

3.6. Echo-triggered explosions

Under finely tuned experimental conditions, a large fraction of explosion events are followed by after-pulses. Figure 3.4 shows an example of what is observed with the particle studied in the experiments of Fig.3.3 but with a slightly lower heating power (97 μW), corresponding to an inter-explosion delay of about 1 μs. In contrast to Fig.3.3, the after-pulse of Fig.3.4 occurs at a well-defined delay of about 200 ns after the main explosion, which distinguishes it from the next explosion requiring a fully restored overheated layer. We propose that after-pulses are weaker explosions triggered by sound echoes of the main explosion, reflected from flat interfaces around the nanoparticle (see the scheme in Fig.3.4.c).

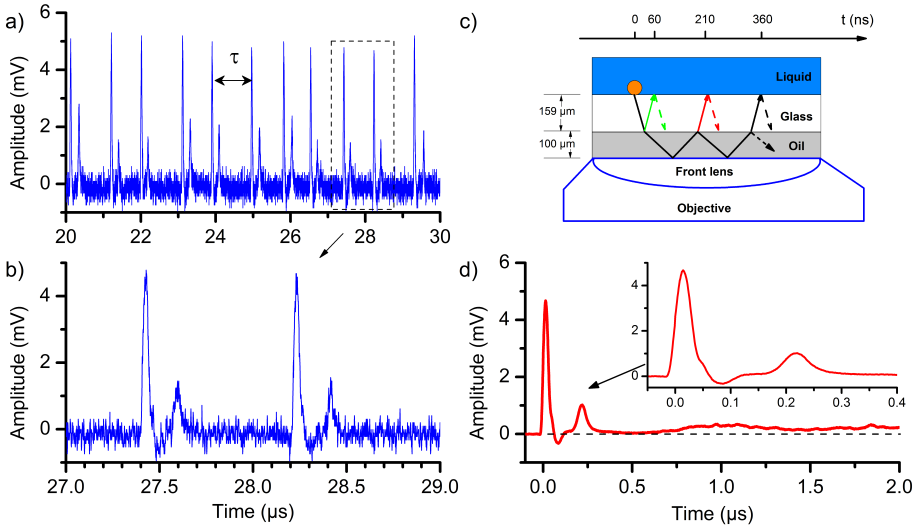

Figure 3.4: Echo-triggered nanobubble explosions under finely-tuned constant heating power above the threshold. (a) The non-averaged time trace of scattered probe presenting echo-triggered bubbles. The probe power is fixed at 5 mW; (b) zoom-in time trace on the dash-block part in (a); (c) space-time scheme showing the sound propagation and reflections in different media around the particle; (d) averaging signal of 1,108 explosions in (a) in the same way as Fig.3.3 (c). Insert: zoom-in on the main peak.

Two interfaces are possible candidates: i) the other side of the glass coverslip. With a thickness of 159 μm and a sound velocity of 5640 m/s [87], the echo arrives 56 ns after the explosion. This is precisely the delay of the shoulder seen in the decay of the bubble signal, both in Fig.3.3 (c) and Fig.3.4 (d); ii) the interface between the immersion oil and the objective lens. The distance between the lens and the oil-glass interface is 100 μm (working distance ac-

cording to the manufacturer). With a sound velocity of 1350 m/s in oil [88], this echo from the second interface should arrive about 204 ns after the main explosion, exactly as observed in Fig.3.4 (d). The after-pulse would thus be a second, weaker explosion triggered by the echo. It may feed on thermal energy left in the hot water layer after the first explosion or conducted from the hot particle. This remarkable phenomenon highlights the extreme sensitivity of a bubble to weak perturbations. Although the initial sound wave is attenuated by two transmissions through the glass-oil interface, reflection on an oil-glass interface and propagation as a spherical wave through 159 μm of glass and 100 μm of oil, this weak echo wave suffices to trigger a measurable signal 56 ns after the first explosion and even a second explosion 204 ns later. In a few cases (see Appendix F), a second after-pulse follows the first one and can be attributed to an additional reflection.

3.7. Towards the stabilization of a nanobubble

The nanobubble around the particle can be stabilized by means of a suitable time profile of the laser intensity. The instable layer of overheated liquid around the nanoparticle makes it impossible to pass smoothly from regime I to regime II mentioned in the introduction. However, the inverse process, in which the heating power is continuously decreased from a point in regime II does not generate any unstable situation. Indeed, the continuous presence of the liquid/vapor interface ensures that the two phases remain in equilibrium at all times, so that the bubble disappears in a continuous way when the heating power is reduced.

We designed the following time profile of the heating laser power to lengthen the nanobubble's persistence. We start just below the critical boiling power (0.96 P_c), then suddenly raise the heating intensity to a high value (1.1 P_c; in practice, due to the finite response time of our acousto-optic modulator, the rise in heating lasts about 100 ns). We then keep the intensity at this high level for a variable duration, 1 μs in the case of Fig.3.5, before reducing it back to the initial level. The result of this cycle for the scattered light is shown in Fig.3.5 together with the heating intensity profile. The measurements were done in liquid pentane.

Averaged probe signal traces following a raise in heating power are presented in Fig.3.5 (see single-shot traces in Appendix G). Again, the individual single-shot traces were averaged by synchronizing them on the mid-rising edge of the probe signal. The averaged trace clearly shows an initial explosion of about 30 ns duration and of lower amplitude than those in Figs.3.3 and 3.4, followed by a plateau at a high scattering value. The probe signal after the ex-

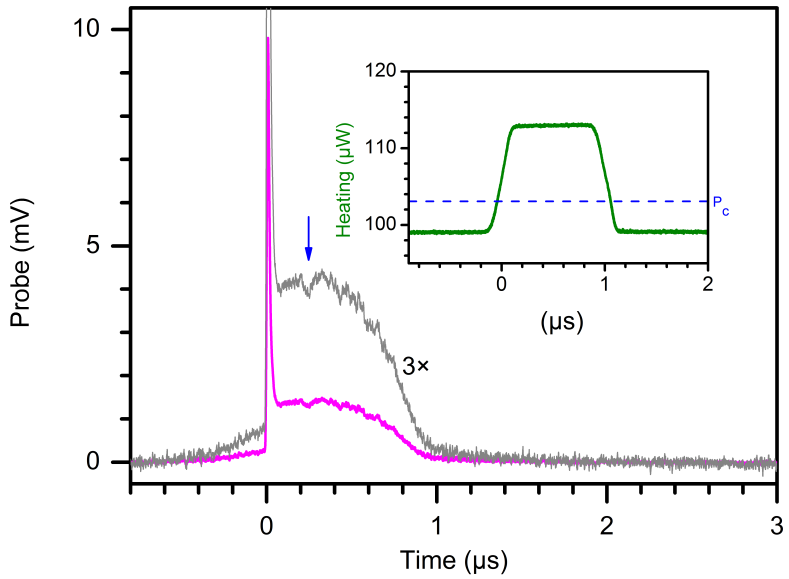

Figure 3.5: Formation of a persistent nanobubble. The pink line shows the probe signal averaged over 200 explosive events following triggering by a raise in heating power. Detector gain: ×10,000, bandwidth: 200 MHz. The events have been averaged by synchronizing at mid-rising edge of the probe transient signal. Insert: The averaged heating profile (green), synchronized at mid-rising edge of the periodic heating pulse as delivered by the acousto-optic modulator. The dashed line is the critical heating power. After explosive formation, the nanobubble persists for up to 800 ns. The heating beam is modulated by a block pulse profile with a frequency of 100 kHz and a duty cycle of 10% (1 μs on-time in a 10 μs period).

plosion is much higher than before, when it was due to the liquid's temperature change alone. This high value indicates the presence of the bubble, and its persistence for as long as the heating power is kept at the high level. The bubble disappears as soon as the heating power is reduced. We therefore conclude that, in the few hundred ns following the explosion, the bubble reaches the steady-state extent discussed and calculated in chapter 2. After the shrinking phase of the initial explosion, the bubble remains as a stable shell because enough heating power is provided, and the energy received by the vapor shell from the particle balances the energy lost by conduction to the cooler liquid outside. This experiment shows the feasibility of reaching and maintaining steady state II, once the barrier of bubble formation is passed. Much longer times than 1 μs could be achieved by optimizing the time profile and intensity stability of the heating power or by a proper, fast enough feedback mechanism from the scat-

tered signal. A reproducible feature (shown with a blue arrow) appears on the trace of Fig.3.5, about 200 ns after the initial explosion. We assign this feature to the reaction of the nanobubble to the sound echo reflected by the oil-lens interface discussed in the previous section.

In some measurements with the same protocol in water, we observed self-oscillations of the nanobubble. Figure 3.6 shows a single-shot observation of a nanobubble formed in water upon a 1 μs raise of heating power. The particle size is still 80 nm in diameter. This bubble appears without an initial explosion and starts to oscillate after a few hundreds of ns. The oscillations damp out when the power is decreased again below the critical value. The oscillation period is roughly consistent with the time given by the Minnaert oscillation period of a bubble [17]. The possible mechanism of this self-oscillation is still unclear and requires additional investigation in the future.

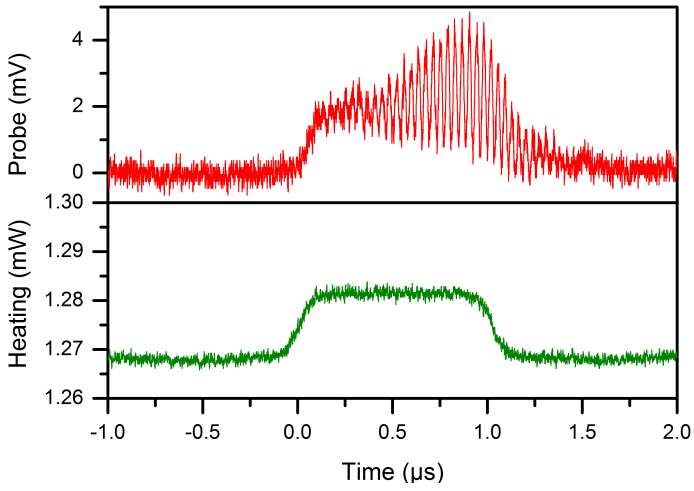

Figure 3.6: A single-shot time trace showing the self-oscillating behavior of a nanobubble. Above: probe signal; Below: heating profile. In this measurement, the gold particle is in pure water and on BK7 glass substrate. The duration of the heating 'pulse' is 1 μs. The oscillation period of the bubble is about 30 ns, corresponding to 33 MHz.

3.8. Conclusions and outlook

Boiling of a liquid around a heated metal nanoparticle can be controlled and detected with high sensitivity and fast time response. Even under continuous-wave heating, nanobubble formation is explosive. No after-bounce could be detected upon bubble shrinking, presumably because all kinetic energy is dis-

sipated upon vapor condensation. The fast time response (less than 15 ns for the expansion and 20-30 ns for the contraction) could be used for all-optical light modulation with a bandwidth of about 100 MHz, several orders of magnitude faster than with liquid crystals [76]. Within a narrow range of heating power, the nanobubble becomes extremely sensitive to weak perturbations such as sound waves reflected from far-away interfaces. Acoustic wave fronts released in an initial explosion could trigger a new explosion, or even lead to self-oscillations. We have shown that a steam nanobubble can be stabilized with a suitable heating intensity profile, and by controlling the heating laser power during the shrinking phase.

In this work, we did not provide a proper theoretical modeling. Compared to the inertial Rayleigh-Plesset theory and its refined versions including surface tension [19] and heat and mass transfer [5], the present system requires consideration of the thermodynamic and kinetic features of the liquid-gas phase transition [16] at nanometer scales. Moreover, the geometry of our experiment excludes spherical symmetry and calls for a full 3D model. Such a complex theory is well beyond the scope of the present work. Our results suggest using bubbles as nanoscale generators and detectors of acoustic waves, much as radars are used at macroscopic scales for electromagnetic waves.

3.9. Acknowledgments

This work is supported by the Foundation for Fundamental Research on Matter (FOM) with funding from NWO. L.H. acknowledges the financial support of China Scholarship Council. Advice from Dr. P. Zijlstra and programming assistance of A. Carattino are kindly acknowledged.